Talanta 199 (2019) 581–589

Contents lists available at ScienceDirect

Talanta

journal homepage: www.elsevier.com/locate/talanta

One-step synthesis of boron-doped graphene quantum dots for fluorescent sensors and biosensor

Shuyan Ge, Jingbo He, Chenxing Ma, Jiyang Liu, Fengna Xi*, Xiaoping Dong

Department of Chemistry, Zhejiang Sci-Tech University, 5 s Avenue, Xiasha Higher Education Zone, Hangzhou 310018, PR China

ARTICLE INFO

Keywords:
Boron-doped graphene quantum dots
Fluorescent detection
Metal ion
Cytochrome C
Phosphote

ABSTRACT

Heteroatom doping can endow graphene quantum dots (GQDs) with various new or improved structural, optical and physicochemical properties. In contrast to the widely reported oxygen, nitrogen or sulfur doping in GQDs, simple and scalable synthesis of boron-doped GQDs (B-GQDs) with high yield and quantum yields remains challenge. In this work, B-GQDs are one-step synthesized and serve as the fluorescence probes for the fabrication of sensors towards Fe^{3+} ion or phosphate (Pi) as well as biosensor towards cytochrome C (Cyt C). The B-GQDs are facile synthesized using one-step bottom-up molecular fusion between 1,3,6-trinitropyrene and borax in sodium hydroxide under hydrothermal process. The synthesis can be performed using large volume autoclave (500 ml) with a high yield of 71%, indicating possibility for gram-scale production of B-GQDs. The as-prepared B-GQDs exhibit single or bilayer graphene structure, high crystallinity, uniform size, bright (absolute photoluminescence quantum yield of 16.8%) and excitation-independent green fluorescence (maximum excitation wavelength and emission wavelength of 480 nm and 520 nm, respectively). Successful doping of B atoms in the lattice of GQDs enables high selectivity towards Fe^{3+}. Based on quenching of fluorescence of B-GQDs by Fe^{3+} (turn-off model), detection of Fe^{3+} (with limit of detection-LOD of 31.2 nM) and Fe^{3+}-rich Cyt C (with LOD of 5.9 μg/ml) are demonstrated. As Pi can recover Fe^{3+}-quenched fluorescence of B-GQDs (turn-off-on model), indirect fluorescent detection of Pi is also achieved with LOD of 340 nM. In addition, detection of Fe^{3+}, Cyt C and Pi in real samples is achieved.

1. Introduction

Fast, convenient, sensitive and cost-effective detection of physical and environmental small-molecules and macromolecules is crucial in biological, clinic, environmental and industrial fields [1–4]. For instance, Fe^{3+} ion, one of the most essential metals in biological system, plays indispensable roles in physiological and pathological processes because it serves as a fundamental structure of hemoglobin, myoglobin, haemenzymes and co-cofactor of in enzyme [2,5–8]. However, exceeding concentration of Fe^{3+} is associated with severe disorders in hepatitis, hemochromatosis, neurodegenerative diseases and organ dysfunction. Phosphate (Pi) is also concerns with physiological processes including phosphorylation, maintenance of phosphate homeostasis, and nutrition balance [9–12]. In addition, Pi is also a convenient tracer to control organic pollution in bodies of water. On the other hand, macromolecules especially proteins are important as functional components in organism. For example, Cytochrome C (Cyt C) usually attached to the inner membrane of mitochondria as a redox heme-protein. As it plays an important role in the oxidative phosphorylation process, level of Cyt C is applied as an indicator of the apoptotic process in the cell [13–16]. Comparing to traditional methods for detecting Fe^{3+}, Cyt C or Pi such as atomic absorption spectroscopy (AAS) [17,18], surface enhanced Raman scattering (SERS) [19,20], mass spectrometry [21], fluorescence sensing offers advantages of simple and rapid operation, possibility for rapid and real-time monitoring, and high sensitivity. In compared with optical sensors based on mesoporous materials modified by organic probes [22,23], mesoscopic membrane sensors [24], thick-film or other nanomaterial-based biosensors [25,26], fluorescence sensors using non-toxic fluorescent probe with facial synthesis, high brightness and good selectivity is simple and convenient [27–29].

Graphene quantum dots (GQDs) are new emerging members of the luminescent carbon family [30–33]. As discovered as a class of zero-dimensional (0D) graphene with one or few layers and tiny lateral size (< 10 nm), GQDs have recently received tremendous interest due to their outstanding properties including remarkable quantum confinement and edge effects, excellent water dispersibility, biocompatibility and high photostability [34–36]. Doping GQDs with heteroatoms

* Corresponding author.
E-mail address: fengnaxi@zstu.edu.cn (F. Xi).

https://doi.org/10.1016/j.talanta.2019.02.098
Received 5 November 2018; Received in revised form 12 February 2019; Accepted 28 February 2019
Available online 01 March 2019
0039-9140/ © 2019 Elsevier B.V. All rights reserved.

(oxygen, boron, nitrogen, sulfur, etc.) have been proven to be effective strategy to modulate their intrinsic electronic, luminescence and reactive properties [37,38]. In contrast to O, N and S, boron (B) atom is relatively difficult to be doped into the framework of GQDs. Though it exhibits comparable atom size to carbon (C) as adjacent neighbor in the periodic table of elements, B possesses quite different electronegativity (2.04 for B *vs* 2.55 for C) [39]. Until now, the established strategies for the synthesis of B-GQDs (B-GQDs) include carbonization of glucose in boric acid [40], hydrothermal cutting B-doped graphene via strong oxidizing acid [41], electrochemical cutting of boracic graphite [42] or graphite rod (in borax solution) through electrolysis [43–46], high-temperature microwave digestion of GO in $Na_2B_4O_7$ solution [47] or microwave treatment of B-doped graphene rods in organic medium [48]. As doping of B atoms into GQDs represents hole doping, it would effectively tune the electronic nature and result in distinctive characteristics. Simple, efficient and scalable synthesis of B-GQDs with high yield and bright fluorescence is highly desirable.

In this work, simple and efficient bottom-up synthesis of B-doped GQDs (B-GQDs) was present for the fabrication of sensors (towards Fe^{3+} ion or phosphate-Pi) and biosensor (towards Cytochrome C-Cyt C). As illustrated in Fig. 1, B-GQDs was synthesized through one-step bottom-up molecular fusion between 1,3,6-trinitropyrene and borax in sodium hydroxide under hydrothermal condition. The synthesis could be performed in large autoclave with 500 ml volume and B-GQDs were obtained in large quantity (0.142 g/per autoclave) with high yield (71%). As B-GQDs exhibit uniform size, bright, excitation-independent fluorescence and Fe^{3+}-quenched emission, sensitive and turn-off detection of Fe^{3+} ion or Fe^{3+}-rich cytochrome C as well as turn-off-on detection of phosphate are demonstrated (Fig. 1).

2. Experimental section

2.1. Materials and reagents

Pyrene, NaOH, 4-(2-hydroxyethyl)-1-piperazineethanesulfonic acid (HEPES), borax, Cytochrome C (Cyt C), sodium phosphate tribasic dodecahydrate were obtained from Aladdin Chemistry Co. Ltd. (China). Aqueous solutions of K^+, Na^+, Ca^{2+}, Mg^{2+}, Zn^{2+}, Ni^{2+}, Co^{2+}, Cr^{3+} were prepared from their chloride salts (Aladdin Chemistry Co. Ltd., China). Aqueous solutions of Ag^+, Cd^{2+} and Pb^{2+} were prepared from their nitrate salts (Shanghai Zhanyun Chemistry Co. Ltd., China). Al^{3+}, Cu^{2+} was prepared from sulfate salts (Wuxi Zhangwang Chemical reagent, China). Standard Fe^{3+} and Hg^{2+} solutions were obtained from National standard materials center (China). All chemicals were of analytical grade and used as received. All aqueous solutions were prepared with ultrapure water (18.2 MΩ cm, Milli-Q, Millipore).

2.2. One-step synthesis of B-GQDs and characterization

B-GQDs were synthesized through one-step bottom-up molecular fusion between 1,3,6-trinitropyrene (carbon source) and borax (dopant) in sodium hydroxide (alkaline medium) under hydrothermal condition (Fig. 1). Briefly, 1,3,6-Trinitropyrene (2 mg/ml) and borax (0.131 M) were dispersed in NaOH solution (0.125 M, 100 ml) with ultrasonic treatment for 0.5 h before transferred to the hydrothermal autoclave (500 ml) for hydrothermal reaction. To optimize the preparation conditions, different reaction temperatures (120 °C, 140 °C, 160 °C, 180 °C, 200 °C), reaction time (2 h, 4 h, 6 h, 8 h, 10 h), the concentration of NaOH (0.05 M, 0.125 M, 0.25 M, 0.375 M, 0.5 M) or borax (0.026 M, 0.052 M, 0.078 M, 0.104 M, 0.131 M, 0.156 M) were investigated. The resulting brown solution was dialyzed using dialysis bags with cut-off molecular weight (Mw) of 500 Da and 3500 Da to remove un-reacted small molecules and oversized particles, respectively. The saffron-yellow solution of B-GQDs obtained after dialysis was freeze-dried.

For characterization, fluorescence spectrum of B-GQDs was recorded on an RF-5301PC spectrofluorometer (Shimadzu Corporation, Japan). Fluorescent characteristics of B-GQDs at different pH was investigated (0.1 M acetic acid-sodium acetate buffer for pH 3–5, 0.1 M HEPES buffer for pH 6–8, 0.1 M sodium carbonate-sodium bicarbonate buffer for pH 9–11). To study the size and crystallinity of B-GQDs, transmission electron microscopy (TEM) was conducted with operating voltage of 200 kV on a JEM-2100 transmission electron microscope (JEOL Ltd, Japan). Atomic force microscopic (AFM) images were measured to evaluate the thickness of B-GQDs using tapping mode on Bruker Multimode 8 (Bruker. Inc, USA). The B-GQDs sample was deposited onto freshly-exfoliated mica. To investigate the chemical structure of B-GQDs, elemental analysis of the B-GQDs was performed by X-ray photoelectron spectroscopy (XPS) on a PHI5300 electron spectrometer using 250 W, 14 kV, Mg Ka radiation (PE Ltd, USA). Dynamic light scattering was measured using ZETASIZER Nano-ZS90 (Malvern, UK) to study the aggregation-induced change of particle size.

2.3. Effect of cations, anions and biological molecules on the fluorescence of B-GQDs

B-GQDs solution was diluted with HEPES buffer (0.1 M, pH = 6).

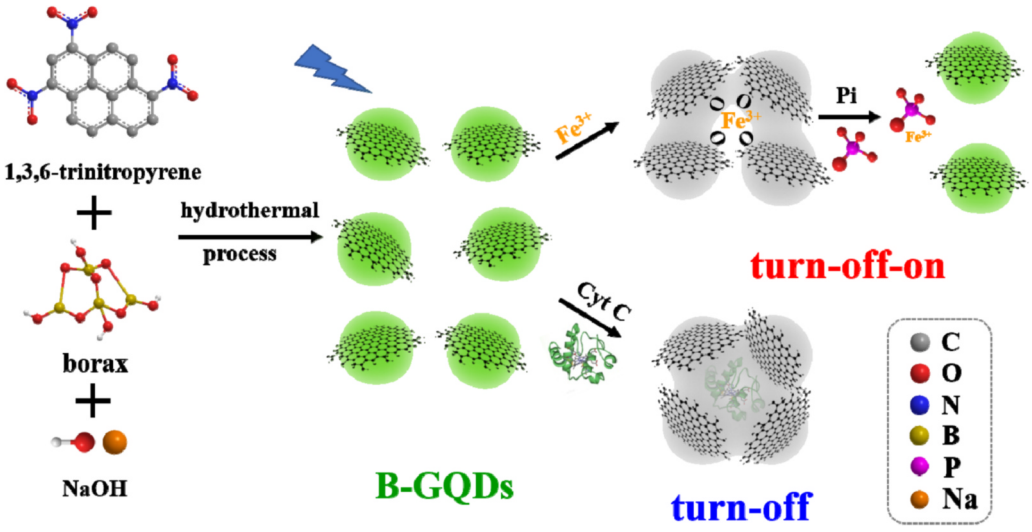

Fig. 1. The illustration of the one-step preparation of B-GQDs for the fabrication of sensors (towards Fe^{3+} ion and phosphate-Pi) and biosensor (towards Cytochrome C-Cyt C).

Solutions of cations (K^+, Na^+, Ca^{2+}, Mg^{2+}, Zn^{2+}, Fe^{3+}, Al^{3+}, Ni^{2+}, Cu^{2+}, Co^{2+}, Cr^{3+}, Pb^{2+}, Cd^{2+}, Ag^+, Hg^{2+}, respectively) or anions (Cl^-, NO_3^-, HCO_3^-, SCN^-, CH_3COO^--AC^-, I^-, NO_2^-, $S_2O_3^{2-}$, $S_2O_8^{2-}$, SO_4^{2-}, PO_4^{3-}, respectively) or biological molecules (Concanavalin A-Con A, bovine albumin-BSA, trypsin, lysozyme-LZM, Cyt C, respectively) were also diluted using the same buffer. After one of cations or anions or biological molecules (500 μM) was added into B-GQDs solution (0.92 mg/ml) and incubated for 10 min, the fluorescence of B-GQDs was observed under UV light (365 nm). The fluorescence intensity of B-GQDs before (F_0) and after (F) addition of metal ions was measured. The fluorescence intensity ratio (F/F_0) was used to evaluate the selectivity.

2.4. Detection of Fe^{3+} or Cyt C using turn-off mode

Detection of Fe^{3+} was proceed in HEPES buffer solution (0.1 M, pH = 6.0). Different concentration of Fe^{3+} (50 nM-420 μM) was added in B-GQDs aqueous (0.23 mg/ml) solution and the resulting solution was incubated for 3 min at room temperature. The fluorescence (FL) intensity of B-GQDs solution in absence and presence of Fe^{3+} was recorded with the excitation wavelength fixed at 480 nm. The relative fluorescence ratio (F/F_0) or fluorescence quenching ratio-(F_0-F)/F_0 were used to evaluate the Fe^{3+}-induced quenching, where F_0 and F represent the FL intensity of the B-GQDs in absence and presence of Fe^{3+}, respectively. For the detection of Fe^{3+} in serum (provided by the second affiliated hospital of medicine, Zhejiang Univ., China), protein-bound Fe^{3+} was firstly released by mixing serum (4 ml) with diluted nitric acid (high-purity, 0.8 M, 4 ml) and stirring for 2 min [37]. After pH was adjusted to 7.0 using NaOH (4 M), the obtained sample was diluted by a factor of 75 using HEPES buffer solution before fluorescent detection. All detections were conducted three times in parallel. Flame atomic absorption spectroscopy (FAAS, PinAAcle 900 T, PE Ltd, USA) were used as the current golden standard to measure the concentration of Fe^{3+} ion in serum [37].

For the detection of Cyt C, similar procedure was adopted with the change of the concentration range (10 μg/ml to 2000 μg/ml) and incubation time (5 min). The relative fluorescence ratio and fluorescence quenching ratio were also calculated using FL intensity of the B-GQDs in absence (F_0) and presence of Cyt C (F_1). For detection of Cyt C in real sample, serum was directly diluted by a factor of 150 using HEPES buffer solution (pH 6.0). The detection reliability was evaluated using standard addition method. A defined amount of Cyt C was added and the obtained samples with artificial concentrations were determined.

2.5. Detection of Pi using turn-off-on mode

Indirect detection (turn-off-on model) of phosphate was achieved by releasing Fe^{3+}-GQDs aggregates using sodium phosphate tribasic. Firstly, B-GQDs (0.23 mg/ml) were mixed with 420 μM Fe^{3+} to quench the fluorescence. After different concentrations of Pi (3 μM to 40 μM) were added, the recovered FL intensity of the mixed solution was recorded. The relative fluorescence recovery ratio (F_2-F)/F_2 was used to evaluate the FL recovery, where F and F_2 represent the FL intensity of the B-GQD-Fe^{3+} in absence of Pi (F) and in presence of Pi (F_2), respectively. The possible interference caused by common anions (Cl^-, HCO_3^-, NO_3^-, SCN^-, AC^-, I^-, NO_2^-, $S_2O_3^{2-}$, $S_2O_8^{2-}$, SO_4^{2-}, respectively) or amino acids (leucine-Leu, threonine-Thr, alanine-Ala, glutamic-Glu, glycine-Gly, tryptophan-Trp, tyrosine-Tyr, respectively) were investigated by adding one of those substrates (60 μM) into B-GQDs-Fe^{3+} system. Then, the recovered FL intensity of the mixed solution was recorded. The environmental sample was obtained from the lake in Zhejiang Sci-Tech University (Xiasha, Hangzhou, China). After filtered using a 0.22 μm membrane to remove large solids and main impurities, the river water was diluted by 12 times using HEPES buffer solution (0.1 M, pH 6.0).

3. Results and discussion

3.1. One-step synthesis and characterization of B-GQDs

In present work, B-GQDs were synthesized through one-step bottom-up molecular fusion between 1,3,6-trinitropyrene and borax in sodium hydroxide under hydrothermal condition (Fig. 1). As 1,3,6-trinitropyrene possesses parent nucleus structure of graphene, it acts as an ideal precursor for the construction of high-quantity GQDs through molecular fusion. In addition, nitro groups will leave in the alkaline medium during the hydrothermal process and provide potential for the introduction of functional groups or heteroatom. To obtain B-GQDs with the highest FL properties, the preparation condition including the reaction time and temperature of the hydrothermal process, as well as the concentration of dopant and alkaline medium were optimized (Fig. S1 in SI). As displayed in Fig. S1A and S1B, the reaction time and temperature affect the FL signal of the obtained material. The increase of reaction time (from 2 to 6 h) in the first stage results in an obvious increase of FL signal due to the accumulation of molecular fusion reaction. On the other hand, the excessive reaction time (8–10 h) weakens the FL intensity, that might be ascribed to the formation of large particles due to possible carbonization. Thus, 6 h was chosen for further investigation. High temperature results in high FL intensity, indicating the effectiveness of forming GQDs by molecular fusion at high temperatures. Considering the safe temperature of the most conventional autoclave, 200 °C was chosen as the optimal reaction temperature (Fig. S1B in SI). As illustrated in Fig. S2C and D, optimal concentration of NaOH and borax were set at 0.125 M and 0.131 M when plateau of FL intensity appeared (Fig. S1C, D in SI). A large quantity of B-GQDs (0.142 g/per autoclave) with high yield of 71% was obtained.

Fig. 2A illustrates the transmission electron microscopic (TEM) images of B-GQDs. Well-distributed B-GQDs with average diameter of 2.0 nm are observed. High-resolution TEM (HRTEM) image (inset of Fig. 2A) reveals the good crystallinity of the B-GQDs with a lattice parameter of 0.24 nm, that is related to the (100) lattice of graphene [35]. As uncovered by atomic force microscopy (AFM) image, B-GQDs exhibit a thickness of 0.9–1.1 nm (Fig. 2B). That indicates single or bilayer of graphene. The composition of the as-prepared B-GQDs was further investigated by X-ray photoelectron spectroscopy (XPS). As shown in Fig. 2C, the XPS survey spectrum of B-GQDs confirms the presence of C, O and B with an atomic concentration of 64.5%, 31.3% and 4.2%, respectively. In the high resolution spectrum of C_{1s}, the binding energy peak at 284.6 eV displays the sp^2 structure of C = C of graphene. The peaks at 283.9 eV, 284.6 eV, 287.5 eV could be respectively assigned to C-B, C = C and C-O (Fig. 2D) [35,49,50]. The high-resolution O_{1s} spectrum (Fig. 2E) revealed the presence of –OH (531.4 eV) [35], B-O groups (532.4 eV) [51], indicating rich oxygen-containing groups on B-GQDs. The B 1s spectrum of B-GQDs shows three peaks around at 189.8, 190.6 and 191.3 eV which can be ascribed to the C-B, BC_2O, and BCO_2 bands (Fig. 2F) [45], indicating successful doping of B atoms in the skeleton of graphene quantum dots. The XRD pattern of the B-GQDs shows a diffraction peak (2θ) at ~25.8° (Fig. S2), corresponding to the (002) plane of graphite.

Due to the strong quantum effect and edge effect, B-GQDs exhibit strong fluorescence (Fig. 3A). As shown, B-GQDs aqueous solution displayed the pale-yellow under visible light and emitted green fluorescence under UV light (inset of Fig. 3A). When the excitation wavelength increased from 400 nm to 485 nm, the FL emission intensity of B-GQDs increased with unchanged emission center, indicating excitation-independent emission due to uniform size and structure. The maximum excitation wavelength and emission wavelength were 480 nm and 520 nm, respectively. Three B-GQDs samples prepared independently exhibit the same fluorescent spectrum with a relative standard deviation (RSD) of 3.2% in fluorescent intensity (at the maximum emission of 520 nm). The absolute photoluminescence quantum yield (QY) of B-GQDs was 16.8%. In compared with that of OH-GQDs (23.2%) that

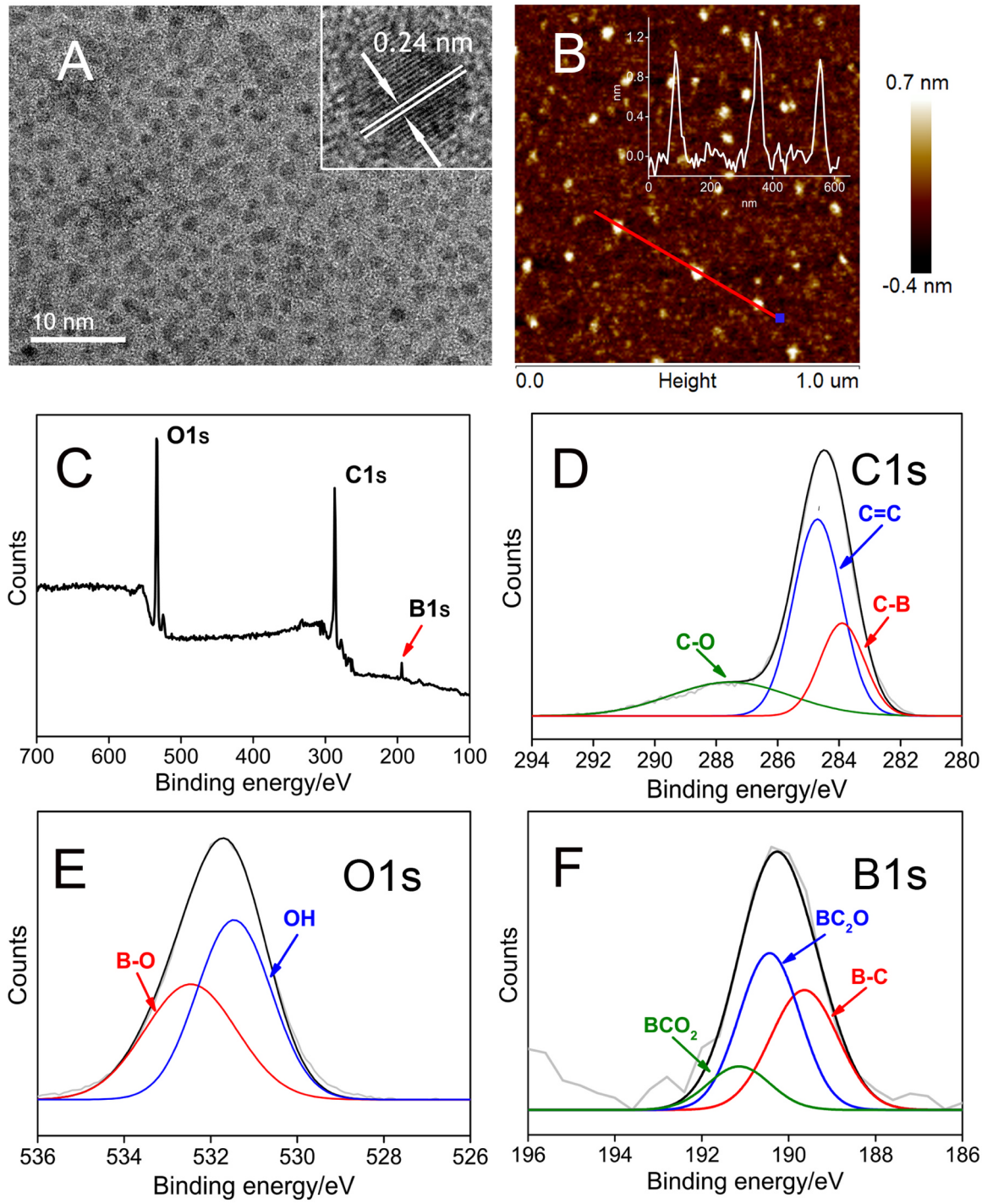

Fig. 2. (A) TEM image of B-GQDs. The inset is the high-resolution TEM (HRTEM) image with resolved crystalline lattice of B-GQDs. (B) AFM image of B-GQDs. Inset is the corresponding height profiles along the indicated line. (C) Full-scan XPS spectrum and high-resolution (D) C 1s, (E) O 1s and (F) B 1s spectra of B-GQDs.

were synthesized without addition of B dopant, the decrease of QY might be due to the doping of B because B atom possesses lower electronegativity and exhibits electron-withdrawing characteristic. The effect of pH (from 3 to 11) on FL intensity of B-GQDs was investigated (Fig. 3B). As revealed, B-GQDs had bright fluorescence under alkaline conditions, whereas, the FL intensity at acidic medium (pH < 6) is low, suggesting the change of electronic state at low pH due to the ionization of oxygen-containing groups. The lifetime of B-GQDs (Fig. 3C) is 4.2 ns. As seen from Fig. S3, the FL intensity of B-GQDs remains 90% after continuous irradiation under UV lamp for 3 h, indicating good anti-photobleaching property.

The expanding of synthesis scale of GQDs now remains challenge because the increased heterogeneity in structure and size. Thus, small autoclave (50 ml or 100 ml) is commonly applied and thus small amount of GQDs is obtained. Combination the high yield (0.142 g/batch synthesis) and excellent characteristics (single or bilayer graphene structure, high crystallinity, uniform size, bright and excitation-independent fluorescence) of B-GQDs, the developed method for the synthesis of B-GQDs exhibits potential for gram-scale production.

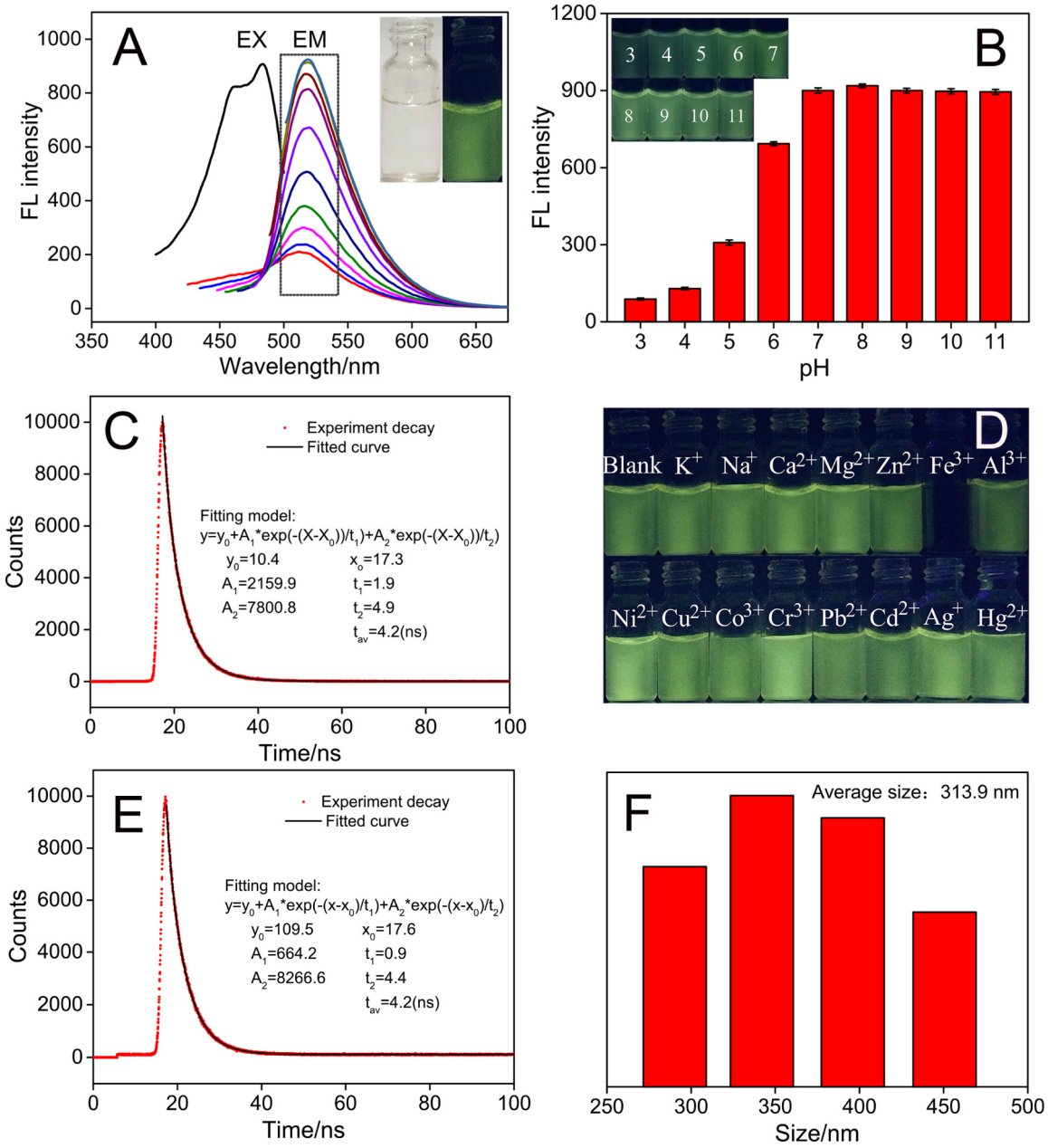

Fig. 3. (A) FL excitation (EX, at emission wavelength of 520 nm) and emission (EM, excitation wavelength increased from 400 to 485 nm with 10 nm increase between adjacent spectra and excitation wavelength of 485 nm of the top spectrum) spectra of the B-GQDs (0.23 mg/ml). Inset represents the photographs of B-GQDs (0.92 mg/ml) under visible (left) and UV (right, 365 nm) lights. (B) The effect of pH on the FL intensity of B-GQDs (0.23 mg/ml). Inset represents the photographs of B-GQDs (0.92 mg/ml) at different pH (indicated in the photographs) under UV light (365 nm). (C) FL lifetime spectrum of B-GQDs (0.92 mg/ml). (D) Photographs of B-GQDs solution (0.92 mg/ml) in presence of different metal ions (500 μM) under 365 nm UV light. (E) FL lifetime spectrum of B-GQDs (0.92 mg/ml) in presence of Fe^{3+} (420 μM). (F) The size distribution of the B-GQDs (0.92 mg/ml) in the presence of Fe^{3+} (250 μM).

3.2. Fluorescence quenching due to the interaction between B-GQDs and Fe^{3+}

The potential of B-GQDs for the detection of ions is investigated. In comparison with other environmentally or physiologically related cations (including K^+, Na^+, Ca^{2+}, Mg^{2+}, Zn^{2+}, Fe^{3+}, Al^{3+}, Ni^{2+}, Cu^{2+}, Co^{2+}, Cr^{3+}, Pb^{2+}, Cd^{2+}, Ag^+, Hg^{2+}, Fig. 3D) and anions (including Cl^-, NO_3^-, HCO_3^-, SCN^-, AC^-, I^-, NO_2^-, $S_2O_3^{2-}$, $S_2O_8^{2-}$, SO_4^{2-}, Pi, Fig. S4 in SI), the fluorescence of B-GQDs could only be obviously quenched by Fe^{3+}, indicating the potential for detection of Fe^{3+} ion. The lifetime of B-GQDs in presence of Fe^{3+} is determined to investigate the quenching mechanism. A life time of 4.2 ns is observed (Fig. 3E), suggesting no transfer of electron occurs during the quenching. However, the aggregation of B-GQDs in presence of Fe^{3+} was revealed by particle size measurement using dynamic light scattering (Fig. 3F) and TEM characterizations (Fig. S5 in SI). As GQDs have ultrasmall nanodiamater, they are quite sensitive to that aggregation and demonstrate fluorescent quenching. It is supposed that Fe^{3+} can coordinate with abound oxygen groups (hydroxyl or B-O) on the surface of B-GQDs to bridge neighboring GQDs together and results in large aggregates, as illustrated in Fig. 1. The non-doping GQDs was also synthesized using the same procedure except the addition of dopant. The selectivity of those non-doping GQDs is also given for comparison. As shown in Fig. S6 (SI), Fe^{3+}-quenched fluorescence is also observed. However, remarkable quenching is observed for both Al^{3+} and Hg^{2+}. Obviously, heteroatom doping changes electronic and structural properties of GQDs and results in selectivity.

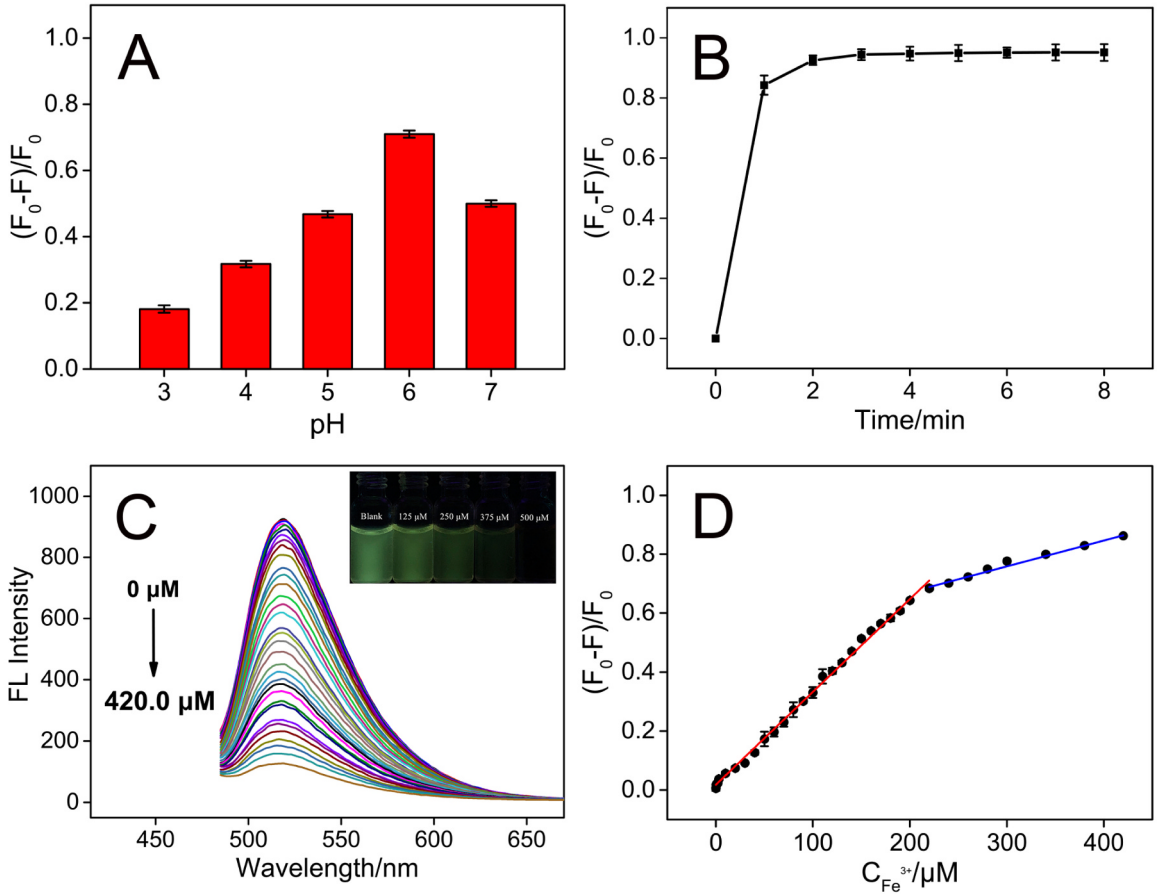

Fig. 4. (A) The effect of pH on FL quenching ration of B-GQDs (0.23 mg/ml) in presence of Fe^{3+} (250 μM). (B) Time-dependent FL response of B-GQDs (0.23 mg/ml) upon the addition of Fe^{3+}. (C) FL spectra of B-GQDs (0.23 mg/ml) upon addition of different concentration of Fe^{3+} in buffered at pH = 6 (HEPES). Inset represents the photographs of B-GQDs (0.92 mg/ml) interacted with different concentrations (indicated in the photographs) of Fe^{3+} under UV light (365 nm). (D) Linear dose response curve for the detection of Fe^{3+}.

3.3. Detection of Fe^{3+} using B-GQDs as fluorescent probe

As B-GQDs exhibit specific recognition for Fe^{3+}, they are applied as fluorescent probe for sensing of Fe^{3+}. To achieve the highest sensitivity, the detection conditions including pH and incubation time were optimized. As Fe^{3+} was easily hydrolyzed to form hydroxides under alkaline conditions, we only investigated the interaction between B-GQDs and Fe^{3+} in acidic or neutral conditions by calculating the relative fluorescence quenching ratio. As shown in Fig. 4A, the highest fluorescence quenching exist at pH = 6. At the same time, fast kinetics was observed because the plateau of fluorescence quenching appeared within 3 min (Fig. 4B). Under those optimal detection conditions, fluorescent spectra of B-GQDs towards different concentration of Fe^{3+} are shown in Fig. 4C. Linear detection of Fe^{3+} ranged from 50 nM to 220 μM ($y = 0.00315\,C + 0.01801$, $R^2 = 0.9984$) and 220 μM to 420 μM ($y = 0.000878\,C + 0.49513$, $R^2 = 0.9973$) was observed. The detection limit was calculated to be 31.2 nM at a signal-to-noise ratio of 3(Fig. 4D). The LOD is lower than those obtained using GQDs [52,53] (N-GQDs) [54,55] and GQDs/polystyrenic anion-exchange resin [56], amino acid- GQDs [57], and glutathione-doped GQDs [58].

B-GQDs were further applied as a fluorescent probe to detect the content of Fe^{3+} in serum. The obtained result (18.10 ± 0.39 μM, n = 3) is in accordance with those obtained (18.54 ± 0.43 μM, n = 3) using flame atomic absorption spectroscopy (FAAS). As FAAS requires bulky instrument and high operation skills, our B-doped GQDs is simple, fast and convenient.

3.4. Fluorescent detection of Cyt C with B-GQDs being fluorescent probe

Though GQDs can offer significant advantages for biosensing due to good biocompatibility, excellent dispersity in aqueous solution and stability against photobleaching, GQDs-based biosensors without complex modification GQDs through specific ligands is less reported. We found that the fluorescence of B-GQDs can be strongly quenched by cytochrome C (Cyt C), indicating specific interaction between B-GQDs and Cyt C. On the contrary, the commonly biological macromolecules including concanavalin A (Con A), bovine serum albumin (BSA), trypsin, and lysozyme (LZM) do not quench the fluorescence of B-GQDs (Fig. S7 in SI), illustrating the selectivity of B-GQDs towards Cyt C. The highest quenching ratio caused by Cyt C (Fig. 5A) appears at pH 6.0 with fast kinetic of 5 min. The possible mechanism for the quenching was investigated. The lifetime of B-GQDs in presence Cyt C is revealed to be 4.2 ns (Fig. 5B), that agrees well with the lifetime of B-GQDs, indicating no charge transfer and exciton recombination process of B-GQDs in the presence of Cyt C. Fig. 5C displayed the ultraviolet (UV) absorption spectrum of Cyt C. As shown, characteristic adsorption peak at ~520 nm is observed that is similar with the emission peak of B-GQDs. Thus, the emitted light by fluorescent emission of B-GQDs can be adsorbed by Cyt C, that could result in the fluorescent quenching. In addition, the aggregation of B-GQDs in presence of Cyt C is further proven by DLS (Fig. 5D). The aggregates also contribute to the fluorescent quenching of B-GQDs. Even when trypsin, a hydrolase that can effectively degrade Cyt C, was added in the mixture of B-GQDs and Cyt C, no FL recovery is observed. Thus, we hypothesis that B-GQDs interact with Cyt C through Fe^{3+} as Cyt C is a Fe^{3+}-rich protein. Hence the

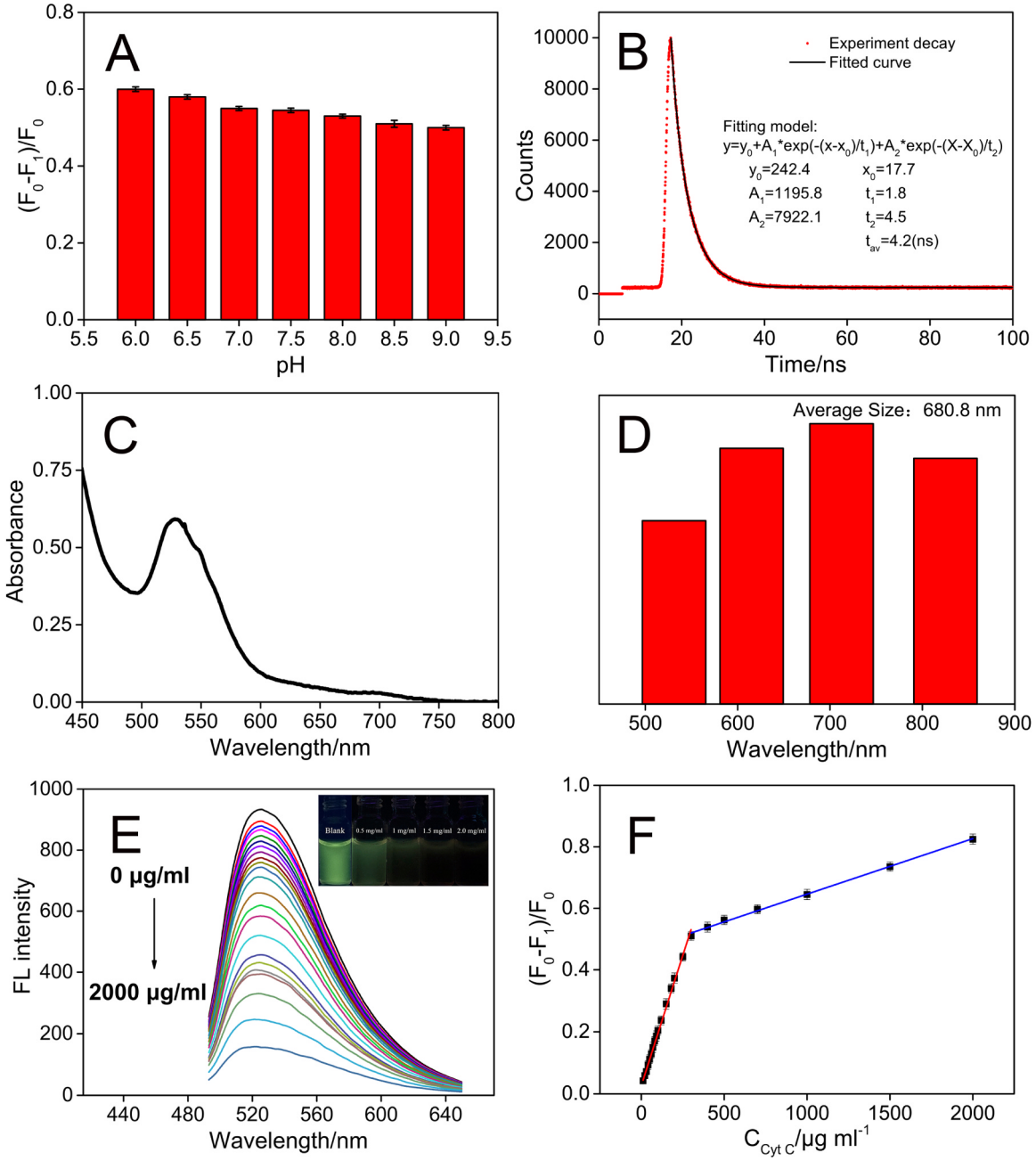

Fig. 5. (A) The FL quenching ratio of B-GQDs (0.23 mg/ml) at different pH values in presence of Cyt C (700 μg/ml). (B) FL lifetime spectrum of B-GQDs (0.92 mg/ml) in presence of Cyt C (2 mg/ml). (C) The ultraviolet (UV) absorption spectrum of Cyt C (1 mg/ml). (D) The size distribution of the B-GQDs (0.92 mg/ml) in the presence of Cyt C (2 mg/ml). (E) FL spectra of B-GQDs (0.23 mg/ml) upon addition of different concentration of Cyt C in buffered at pH = 6 (HEPES). Inset represents the photographs of B-GQDs (0.92 mg/ml) interacted with different concentrations (indicated in the photographs) of Cyt C under UV light (365 nm). (F) Linear dose response curve for the detection of Cyt C.

fluorescent detection of Cyt C using B-GQDs as fluorescent probe is demonstrated in Fig. 5E. The fluorescence quenching ratio $(F_0\text{-}F)/F_0$ linearly changed with the concentration of Cyt C ranged from 10–300 μg/ml ($y = 0.00168\,C + 0.02687$, $R^2 = 0.9986$) and 300–2000 μg/ml ($y = 0.0001806\,C + 0.4654$, $R^2 = 0.9987$). The detection limit was calculated to be 5.9 μg/ml at a signal-to-noise ratio of 3 (Fig. 5F). Diluted serum samples with artificially spiking in a defined amount of Cyt C were examined by B-GQDs based fluorescent sensor. As shown in Table S1, the recovery (agreement between measurements and the pre-set concentrations) of our sensor is satisfactory (between 95.4% and 97.2%) with low relative standard deviation (RSD, between 1.1% and 2.2%).

3.5. Fluorescent detection of Pi using turn-off-on model

As phosphate is well-known reagent that can coordinate with Fe^{3+}, we next demonstrate that B-GQDs-Fe^{3+} complex can be employed to establish a turn-on FL sensing of Pi. As revealed in Fig. 1, the initial fluorescence of B-GQDs could de quenched by formation aggregates in presence of Fe^{3+}. When Pi is added in the mixture of B-GQDs and Fe^{3+} ion, fluorescent recovery is observed, indicating the dissociation of B-GQDs from the aggregates and re-dispersion as free phosphor. As demonstrated in Fig. 6A, the fluorescence recovery ratio is linearly increased with the concentration of Pi from 3 to 40 μM ($y = 0.01503\,C + 0.0402$, $R^2 = 0.9988$). The detection limit was calculated to be 340 nM (s/n = 3). The selectivity for Pi-induced FL recovery

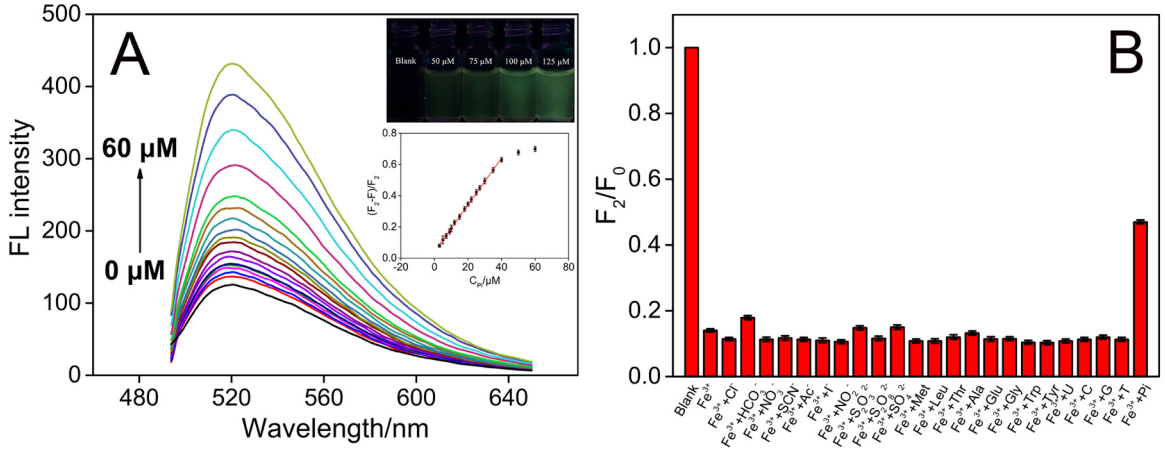

Fig. 6. (A) FL spectra of B-GQDs (0.23 mg/ml) with Fe^{3+} (420 μM) and different concentration of phosphate (Pi). Inset (top) represents the photographs of B-GQDs (0.92 mg/ml) + Fe^{3+} (420 μM) solution interacted with different concentrations (indicated in the photographs) of Pi under UV light (365 nm). Inset (below) is the linear dose response curve for the detection of Pi. (B) Relative fluorescence ratio (F_2/F_0) in presence of different anions or amino acids (60 μM) in B-GQDs-Fe^{3+} mixture.

was further investigated. The FL recovery by commonly existed anions or amino acids was given in Fig. 6B. In comparison with Pi that can strongly recovers the fluorescence of B-GQDs, the tested ions or amino only exhibit slight effect on FL recovery, indicating good selectivity by phosphote. In addition, those anions or amino acids (Fig. S8A in SI) or their binary mixture (Fig. S8B in SI) do not interfere the recovered fluorescence of B-GQDs by Pi. Lake waters with artificially spiking in a defined amount of Pi were also detected using B-GQDs based fluorescent sensor. As shown in Table S2, the recovery is satisfactory (between 97.0% and 101.2%) with low RSD (between 1.8% and 3.4%).

4. Conclusion

Boron doped graphene quantum dots (B-GQDs) were simply synthesized using a facile one-step hydrothermal process. B-GQDs exhibit single or bilayer graphene structure, high crystallinity, uniform size, bright and excitation-independent fluorescence. Taking the advantages of high yield and excellent characteristics, the developed strategy for the synthesis of B-GQDs exhibits potential for gram-scale production. Successful doping of B atoms enables high selectivity towards Fe^{3+} ion. Based on the direct fluorescence quenching (turn-off model), B-GQDs are employed to sensitive detect Fe^{3+} or Fe^{3+}-containing protein. In addition, indirect detection of phosphate is achieved as it can recover the fluorescence of B-GQDs quenched by Fe^{3+}. Finally, we demonstrate that this B-GQD sensors can be used for complex samples, suggesting its potential for practical use.

Acknowledgements

We acknowledge the financial support from the Zhejiang Provincial Natural Science Foundation of China (Nos. LY19B050008 and LY17B050007).

Appendix A. Supporting information

Supplementary data associated with this article can be found in the online version at doi:10.1016/j.talanta.2019.02.098.

References

[1] X.T. Zhang, A. Ananthanarayanan, K.Q. Luo, P. Chen, Glowing graphene quantum dots and carbon dots: properties, syntheses, and biological applications, Small 11 (2015) 1620–1636.
[2] C. Xia, X. Hai, X.W. Chen, J.H. Wang, Simultaneously fabrication of free and solidified N, S-doped graphene quantum dots via a facile solvent-free synthesis route for fluorescent detection, Talanta 168 (2017) 269–278.
[3] M.R. Saidura, A.R. Abdul Aziza, W.J. Basirun, Recent advances in DNA-based electrochemical biosensors for heavy metal ion detection: a review, Biosens. Bioelectron. 90 (2017) 125–139.
[4] B. Peng, L. Tang, G.M. Zeng, Y.Y. Zhou, Y. Zhang, B.Q. Long, S.Y. Fang, S. Chen, J.F. Yu, Current progress in aptasensors for heavy metal ions based on photoelectrochemical method: a review, Curr. Anal. Chem. 14 (2018) 4–12.
[5] L. Chen, C.L. Wu, P. Du, X.W. Feng, P. Wu, C.M. Cai, Electrolyzing synthesis of boron-doped graphene quantum dots for fluorescence determination of Fe^{3+} ions in water samples, Talanta 164 (2017) 100–109.
[6] T.V. Tam, N.B. Trung, H.R. Kim, J.S. Chung, W.M. Choi, One-pot synthesis of N-doped graphene quantum dots as a fluorescent sensing platform for Fe^{3+} ions detection, Sens. Actuators B 202 (2014) 568–573.
[7] Z.G. Liu, J.C. Xiao, X.W. Wu, L.Q. Lin, S.H. Weng, M. Chen, X.H. Cai, X.H. Lin, Switch-on fluorescent strategy based on N and S co-doped graphene quantum dots (N-S/GQDs) for monitoring pyrophosphate ions in synovial fluid of arthritis patients, Sens. Actuators B 229 (2016) 217–224.
[8] M. Shamsipur, K. Molaei, F. Molaabasi, M. Alipour, N. Alizadeh, S. Hosseinkhani, M. Hosseini, Facile preparation and characterization of new green emitting carbon dots for sensitive and selective off/on detection of Fe^{3+} ion and ascorbic acid in water and urine samples and intracellular imaging in living cells, Talanta 183 (2018) 122–130.
[9] H.X. Zhao, L.Q. Liu, Y. Wang, X.J. Zhao, C.Z. Huang, Highly selective detection of phosphate in very complicated matrixes with an off–on fluorescent probe of europium-adjusted carbon dots, Chem. Commun. 47 (2011) 2604–2606.
[10] B.B. Chen, R.S. Li, M.L. Liu, H.Y. Zou, H. Liu, C.Z. Huang, Highly selective detection of phosphate ion based on a single-layered graphene quantum dots-Al^{3+} strategy, Talanta 178 (2018) 172–177.
[11] J.M. Bai, L. Zhang, R.P. Liang, J.D. Qiu, Graphene quantum dots combined with europium ions as photoluminescent probes for phosphate sensing, Chem. Eur. J. 19 (2013) 3822–3826.
[12] S. Sun, K. Jiang, S.H. Qian, Y.H. Wang, H.W. Lin, Applying carbon dots-metal ions ensembles as a multichannel fluorescent sensor array: detection and discrimination of phosphate anions, Anal. Chem. 89 (2017) 5542–5548.
[13] X.L. Zhang, Z.R. Tang, Y.P. Dong, C.M. Wang, Electrogenerated chemiluminescence of ZnO nanorods and its sensitive detection of cytochrome C, Talanta 179 (2018) 139–144.
[14] H.J. Zhang, B.X. Zhang, C.X. Di, M.C. Ali, J. Chen, Z. Li, J. Si, H. Zhang, H.D. Qiu, Label-free fluorescence imaging of cytochrome c in living systems and anti-cancer drug screening with nitrogen doped carbon quantum dots, Nanoscale 10 (2018) 5342–5349.
[15] N. Wang, A.Q. Zheng, X. Liu, J.J. Chen, T. Yang, M.L. Chen, J.H. Wang, Deep eutectic solvent-assisted preparation of nitrogen/chloride-doped carbon dots for intracellular biological sensing and live cell imaging, ACS Appl. Mater. Interfaces 10 (2018) 7901–7909.
[16] L. Cao, X.Q. Li, L.X. Qin, S.Z. Kang, G.D. Li, Graphene quantum dots supported by graphene oxide as a sensitive fluorescence nanosensor for cytochrome c detection and intracellular imaging, J. Mater. Chem. B 5 (2017) 6300–6306.
[17] S. Gil, I. Lavilla, C. Bendicho, Ultrasound-Promoted cold vapor generation in the presence of formic acid for determination of mercury by atomic absorption spectrometry, Anal. Chem. 78 (2006) 6260–6264.
[18] G. Chakrapani, P.L. Mahanta, D.S.R. Murty, B. Gomathy, Preconcentration of traces of gold, silver and palladium on activated carbon and its determination in geological samples by flame AAS after wet ashing, Talanta 53 (2001) 1139–1147.
[19] S.J. Lee, M. Moskovits, Visualizing chromatographic separation of metal ions on a surface-enhanced raman active medium, Nano Lett. 11 (2011) 145–150.
[20] Y.X. Du, R.Y. Liu, B.H. Liu, S.H. Wang, M.Y. Han, Z.P. Zhang, Surface-Enhanced raman scattering chip for femtomolar detection of mercuric ion (II) by ligand

exchange, Anal. Chem. 85 (2013) 3160–3165.
[21] X. Ran, H.J. Sun, F. Pu, J.S. Ren, X.G. Qu, Ag Nanoparticle-decorated graphene quantum dots for label-free, rapid and sensitive detection of Ag^{+} and biothiols, Chem. Commun. 49 (2013) 1079–1081.
[22] S.A. El-Safty, M.A. Shenashen, Optical mesosensor for capturing of Fe(III) and Hg (II) ions from water and physiological fluids, Sens. Actuators B 183 (2013) 58–70.
[23] M.A. Shenashen, S.A. El-Safty, E.A. Elshehy, M. Khairy, Hexagonal-Prism-Shaped optical sensor/captor for the optical recognition and sequestration of pd^{II} ions from urban mines, Eur. J. Inorg. Chem. 2015 (2015) 179–191.
[24] S.A. El-Safty, M. Khairy, M.A. Shenashen, E. Elshehy, W. Warkocki, M. Sakai, Optical mesoscopic membrane sensor layouts for waterfree and blood-free toxicants, Nano Res. 8 (2015) 3150–3163.
[25] W.C. Mak, C.Y. Chan, J. Barford, R. Renneberg, Biosensor for rapid phosphate monitoring in a sequencing batch reactor (SBR) system, Biosens. Bioelectron. 19 (2003) 233–237.
[26] M. Pandiaraj, T. Madasamy, P.N. Gollavilli, M. Balamurugan, S. Kotamraju, V.K. Rao, K. Bhargava, C. Karunakaran, Nanomaterial-based electrochemical biosensors for cytochrome c using cytochrome c reductase, Bioelectrochemistry 91 (2013) 1–7.
[27] J. Ju, W. Chen, Graphene quantum dots as fluorescence probes for sensing metal ions: synthesis and applications, Curr. Org. Chem. 19 (2015) 1150–1162.
[28] R.B. Xie, Z.F. Wang, W. Zhou, Y.T. Liu, L.Z. Fan, Y.C. Li, X.H. Li, Graphene quantum dots as smart probes for biosensing, Anal. Methods 8 (2016) 4001–4016.
[29] X. Hai, J. Feng, X.W. Chen, J.H. Wang, Tuning the optical properties of graphene quantum dots for biosensing and bioimaging, J. Mater. Chem. B 6 (2018) 3219–3234.
[30] X. Sun, Y.T. Qian, Y.J. Jiao, J.Y. Liu, F.N. Xi, X.P. Dong, Ionic liquid-capped graphene quantum dots as label-free fluorescent probe for direct detection of ferricyanide, Talanta 165 (2017) 429–435.
[31] S.J. Kim, Y.J. Song, M.J. Heller, Polymorphic architectures of graphene quantum dots, Adv. Mater. 29 (2017) 1701845.
[32] L. Lu, L. Zhou, J. Chen, F. Yan, J. Liu, X. Dong, F. Xi, P. Chen, Nanochannel-confined graphene quantum dots for ultrasensitive electrochemical analysis of complex samples, ACS Nano 12 (2018) 12673–12681.
[33] Y.B. Yan, J. Chen, N. Li, J.Q. Tian, K.X. Li, J.Z. Jiang, J.Y. Liu, Q.H. Tian, P. Chen, Systematic bandgap engineering of graphene quantum dots and applications for photocatalytic water splitting CO_2, ACS Nano 12 (2018) 3523–3532.
[34] A. Ananthanarayanan, X.W. Wang, P. Routh, B. Sana, S. Lim, D.H. Kim, K.H. Lim, J. Li, P. Chen, Facile synthesis of graphene quantum dots from 3D graphene and their application for Fe^{3+} sensing, Adv. Funct. Mater. 24 (2014) 3021–3026.
[35] L. Wang, Y.L. Wang, T. Xu, H.B. Liao, C.J. Yao, Y. Liu, Z. Li, Z.W. Chen, D.Y. Pan, L.T. Sun, M.H. Wu, Gram-scale synthesis of single-crystalline graphene quantum dots with superior optical properties, Nat. Commun. 5 (2014) 5357.
[36] N. Li, A. Than, X.W. Wang, S.H. Xu, L. Sun, H.W. Duan, C.J. Xu, P. Chen, Ultrasensitive profiling of metabolites using tyramine-functionalized graphene quantum dots, ACS Nano 10 (2016) 3622–3629.
[37] C. Shen, S.Y. Ge, Y.Y. Pang, F.N. Xi, J.Y. Liu, X.P. Dong, P. Chen, Facile and scalable preparation of highly luminescent N, S co-doped graphene quantum dots and their application for parallel detection of multiple metal ions, J. Mater. Chem. B 5 (2017) 6593–6600.
[38] S.Y. Bian, C. Shen, Y.T. Qian, J.Y. Liu, F.N. Xi, X.P. Dong, Facile synthesis of sulfur-doped graphene quantum dots as fluorescent sensing probes for Ag^{+} ions detection, Sens. Actuators B 242 (2017) 231–237.
[39] X.W. Wang, G.Z. Sun, P. Routh, D.H. Kim, W. Huang, P. Chen, Heteroatom-doped graphene materials: syntheses, properties and applications, Chem. Soc. Rev. 43 (2014) 7067–7098.
[40] T.V. Tam, S.G. Kang, K.F. Babu, E.S. Oh, S.G. Lee, W.M. Choi, Synthesis of B-doped graphene quantum dots as a metal-free electrocatalyst for the oxygen reduction reaction, J. Mater. Chem. A 5 (2017) 10537–10543.
[41] L. Zhang, Z.Y. Zhang, R.P. Liang, Y.H. Li, J.D. Qiu, Boron-doped graphene quantum dots for selective glucose sensing based on the “abnormal” aggregation-induced photoluminescence enhancement, Anal. Chem. 86 (2014) 4423–4430.
[42] Y.M. Zhang, Q. Rong, J.H. Zhao, J. Zhang, Z.Q. Zhu, Q.J. Jiu, Boron-doped graphene quantum dot/Ag-$LaFeO_3$ pp heterojunction for sensitive and selective benzene detection, J. Mater. Chem. A 6 (2018) 12647–12653.
[43] G.C. Yang, C.L. Wu, X.J. Luo, X.Y. Liu, Y. Gao, P. Wu, C.X. Cai, S.S. Saavedra, Exploring the emissive states of heteroatom-doped graphene quantum dots, J. Phys. Chem. C 122 (2018) 6483–6492.
[44] L. Chen, G.C. Yang, P. Wu, C.X. Cai, Real-time fluorescence assay of alkaline phosphatase in living cells using boron-doped graphene quantum dots as fluorophores, Biosens. Bioelectron. 96 (2017) 294–299.
[45] L. Chen, C.L. Wu, P. Du, X.W. Feng, P. Wu, C.X. Cai, Electrolyzing synthesis of boron-doped graphene quantum dots for fluorescence determination of Fe^{3+} ions in water samples, Talanta 164 (2017) 100–109.
[46] Z.T. Fan, Y.C. Li, L.Z. Fan, S.X. Zhou, D.C. Fang, S.H. Yang, Surrounding media sensitive photoluminescence of boron-doped graphene quantum dots for highly fluorescent dyed crystals, chemical sensing and bioimaging, Carbon 70 (2014) 149–156.
[47] X. Hai, Q.X. Mao, W.J. Wang, X.F. Wang, X.W. Chen, J.H. Wang, An acid-free microwave approach to prepare highly luminescent boron-doped graphene quantum dots for cell imaging, J. Mater. Chem. B 3 (2015) 9109–9114.
[48] T.T. Zhang, H.M. Zhao, C.F. Fan, Y.H. Li, L. Li, X. Quan, Electrolytic exfoliation synthesis of boron doped graphene quantum dots: a new luminescent material for electrochemiluminescence detection of oncogene microRNA-20a, Electrochim. Acta 190 (2016) 1150–1158.
[49] S. Sun, L. Zhang, K. Jiang, A.G. Wu, H.W. Lin, Toward high-efficient red emissive carbon dots: facile preparation, unique properties, and applications as multifunctional theranostic agents, Chem. Mater. 28 (2016) 8659–8668.
[50] J. Zhan, B.J. Geng, K. Wu, G. Xu, L. Wang, R.Y. Guo, B. Lei, F.F. Zheng, D.Y. Pan, M.H. Wu, A solvent-engineered molecule fusion strategy for rational synthesis of carbon quantum dots with multicolor bandgap fluorescence, Carbon 130 (2018) 153–163.
[51] B. Buchholcz, E. Varga, T. Varga, K. Plank, J. Kiss, Z. Kónya, Structure and stability of boron doped titanate nanotubes and nanowires, Vacuum 138 (2017) 120–124.
[52] H.B. Xu, S.H. Zhou, L.L. Xiao, S.Z. Li, T. Song, Y. Wang, Q.H. Yuan, Nanoreactor-confined synthesis and separation of yellow-luminescent graphene quantum dots with a recyclable SBA-15 template and their application for Fe (III) sensing, Carbon 87 (2015) 215–225.
[53] X.W. Zhu, Z. Zhang, Z.J. Xue, C.H. Huang, Y. Shan, C. Liu, X.Y. Qin, W.S. Yang, X. Chen, T. Wang, Understanding the selective detection of Fe^{3+} based on graphene quantum dots as fluorescent probes: the Ksp of a metal hydroxide-assisted mechanism, Anal. Chem. 89 (2017) 12054–12058.
[54] H.B. Xu, S.H. Zhou, L.L. Xiao, H.H. Wang, S.Z. Li, Q.H. Yan, Fabrication of a nitrogen-doped graphene quantum dot from MOF-derived porous carbon and its application for highly selective fluorescence detection of Fe^{3+}, J. Mater. Chem. C 3 (2015) 291–297.
[55] J. Ju, W. Chen, Synthesis of highly fluorescent nitrogen-doped graphene quantum dots for sensitive, label-free detection of Fe (III) in aqueous media, Biosens. Bioelectron. 58 (2014) 219–225.
[56] W.J. Zhang, J. Gan, Synthesis of blue-photoluminescent graphene quantum dots/polystyrenic anion-exchange resin for Fe(III) detection, Appl. Surf. Sci. 372 (2016) 145–151.
[57] Q. Ma, J.P. Song, S.Z. Wang, J. Yang, Y. Guo, C. Dong, A general sensing strategy for detection of Fe^{3+} by using amino acid-modified graphene quantum dots as fluorescent probe, Appl. Surf. Sci. 389 (2016) 995–1002.
[58] K. Saenwong, P. Nuengmatcha, P. Sricharoen, N. Limchoowong, S. Chanthai, GSH-doped GQDs using citric acid rich-lime oil extract for highly selective and sensitive determination and discrimination of Fe^{3+} and Fe^{2+} in the presence of H_2O_2 by a fluorescence “turn-off” sensor, RSC Adv. 8 (2018) 10148–10157.